JOURNAL OF GEOPHYSICAL RESEARCH, VOL. 90, NO. B1, PAGES 635-649, JANUARY 10, 1985

STRUCTURE OF THE BENIOFF ZONE BENEATH THE SHUMAGIN ISLANDS, ALASKA: RELOCATION OF LOCAL EARTHQUAKES USING THREE-DIMENSIONAL RAY TRACING

Egill Hauksson[1]

Lamont-Doherty Geological Observatory of Columbia University, Palisades, New York

Abstract. Seismic rays are traced through a prescribed three-dimensional inhomogeneity that simulates the subducted slab below the Shumagin Islands region to calculate local station delays for a given hypocenter and a slab model. Hypocenters determined by the Shumagin seismic network are then relocated using the station delays, a flat-layered velocity structure and a standard earthquake location computer program. Station delays are calculated for 12 hypocenters with respect to six different slab models to identify the slab model that is most consistent with the available arrival time and waveform data. A set of path corrections that is calculated for each grid point-station pair on a preliminary grid of 36 points in the depth range from 60 to 300 km is used to recalculate the hypocenters for all of the 1982 earthquakes with depths greater than 50 km. Application of this method to data from 1982 for the digitally recording Shumagin seismic network shows the following results: (1) a previously observed apparent increase in dip of the subducted slab at depths of ≈ 100 km disappears, (2) the subducted slab can be modeled as a dipping structure that dips at a constant angle of 45° toward north-northwest at depths between 80 and 250-300 km and has a 7% higher velocity than the surrounding mantle, (3) hypocenters determined from Shumagin network data are located only 10-20 km south of high-quality hypocenters determined from teleseismic data alone, (4) qualitative comparison of digitally recorded seismograms with calculated ray paths shows enrichment of high-frequency coda, possible converted phases, and low amplitudes of first P arrivals for rays that travel mostly along the slab. Conversely, for rays that travel almost vertically through the upper plate the seismograms show a high amplitude of first P arrivals that are followed by an insignificant coda and low-amplitude S waves.

Introduction

Along most of the Aleutian arc the Pacific plate is being subducted underneath the North American plate at rates of relative motion of 60-80 mm yr^{-1} [Minster and Jordan, 1978]. This study focuses on the 350-km-long segment of the arc called the Shumagin Islands in the eastern Aleutians (see Figure 1). In several recent papers the structure of the plate interface beneath the Shumagin Islands has been inferred from the spatial distribution of locally recorded earthquakes [Davies and House, 1979; Davies et al., 1981; Reyners and Coles, 1982]. A standard location procedure that is based on a flat-layered velocity distribution was applied to determine the locations of these earthquakes. Since the 6-10% higher velocity of the descending slab (as compared to the surrounding mantle) is not taken into account when determining these hypocenters, they possibly can be mislocated. Hence if the slab effect is taken into account, any interpretations of the position and geometry of the plate boundary based on the hypocentral distribution can be improved significantly.

Jacob [1970], Toksoz et al. [1971], and Sleep [1973] quantified the effects of the lithospheric slabs on travel times and ray paths of downgoing rays to explain observed teleseismic residuals. In the central Aleutians near Adak Island, Engdahl [1973] relocated locally recorded earthquakes, using three-dimensional ray tracing to account for the assumed presence of the slab. He found a 10-km-thick Benioff zone located in the upper part of the downgoing plate. Recently, Spencer and Engdahl [1983] used ray-tracing methods and teleseismically recorded arrival times to constrain the velocity structure in the Adak Island region. They then, in turn, applied the new velocity structure to calculate improved locations of locally recorded earthquakes. They point out that the recalculated hypocenters that are based on locally recorded data are more in agreement with teleseismic locations than the hypocenters found in earlier studies. Independently, Frohlich et al. [1982] showed that the slab effect in the Adak region can bias the epicenters of deep local earthquakes by as much as 80 km. Hasegawa et al. [1978] improved the locations of local earthquakes beneath northern Honshu in Japan using ScS and ScSp phases of distant earthquakes and three-dimensional ray tracing to constrain the position of the subducting slab. Their improved hypocenters form a double-planed Benioff zone that is defined by the spatial distribution of hypocenters as well as by different composite fault plane solutions.

In this study the possible mislocations of hypocenters determined from Shumagin network data are evaluated by incorporating a descending slab of 7% higher velocity than the surrounding mantle into the location procedure. The results from testing six different slab models are then used to derive an improved model of the plate interface beneath the Shumagin Islands in the eastern Aleutians. To test a more general and less time-consuming procedure, a set of path corrections from a grid of points is calculated for each station and used to recalculate the hypocenters of the 1982 earthquakes located deeper than 50 km.

[1]Now at Department of Geological Sciences, University of Southern California, Los Angeles.

Paper number 4B1068.
0148-0227/85/004B-1068$05.00

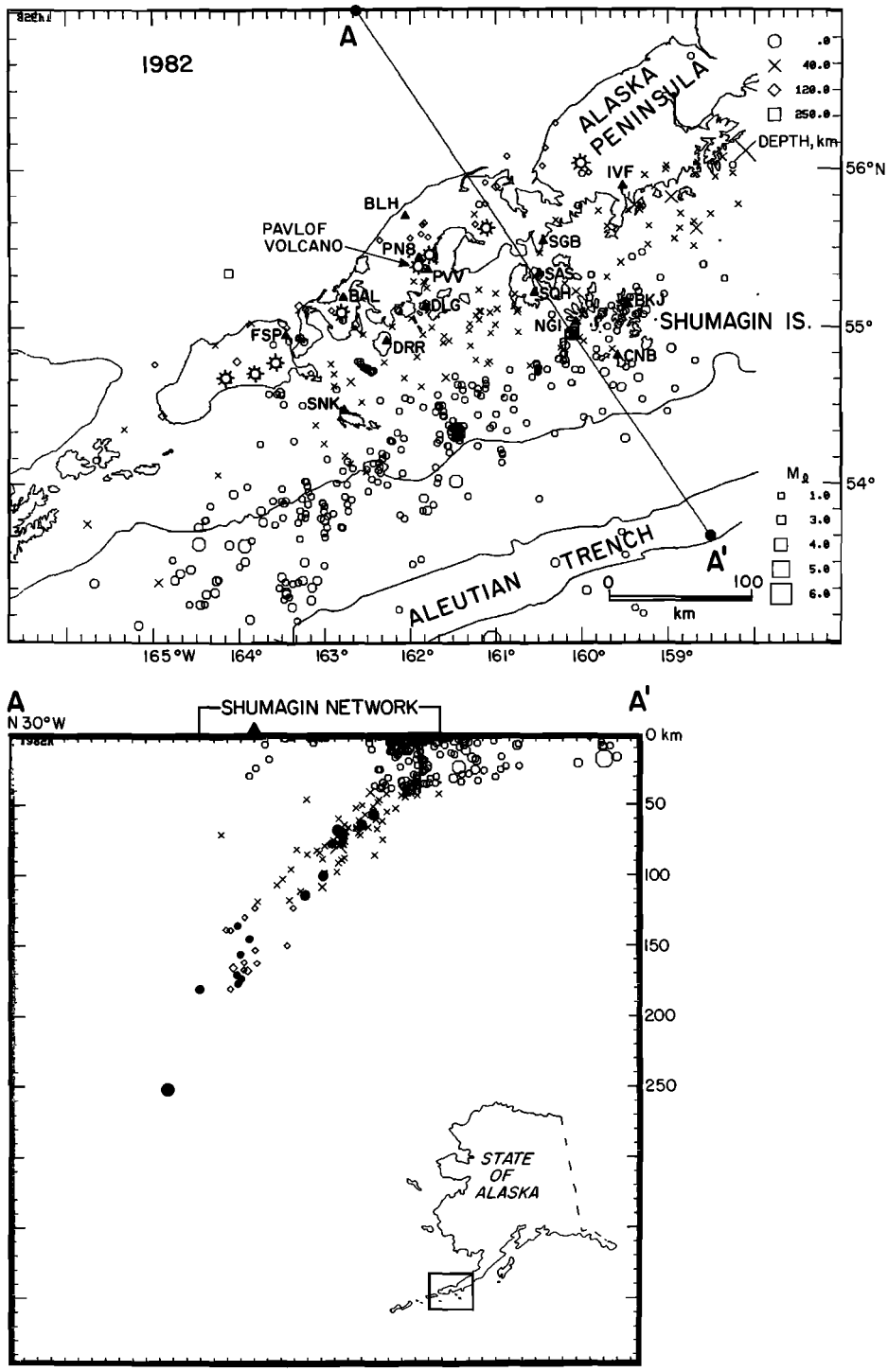

Fig. 1. Seismicity recorded by the Shumagin seismic network in eastern Aleutians, Alaska, during 1982. The location of this map in the eastern Aleutians is indicated in the lower right-hand corner of the cross section. (Top) Map view showing epicenters where symbol type is keyed to depth and symbol size is keyed to magnitude. Seismic stations are designated by a solid triangle and a three-letter code. Stations BLH, PVV, SGB, SAS, and CNB are equipped with three-component seismometers. Active volcanoes on the Alaska Peninsula are shown as marked open circles. (Bottom) Depth cross section with no vertical exaggeration taken along the profile A-A'. The solid circles represent the hypocenters of the 15 earthquakes relocated in this study.

Possible variations in the shallow velocity structure of the upper plate are not included in this study. Although such variations may affect the locations of shallow earthquakes, this study presumes that they have only a small effect on the locations of the deep earthquakes within the subducted slab.

Data and Methods

Initially, the method of relocating the earthquakes as applied in this study was proposed by K. H. Jacob (personal communication, 1981). Independently, Engdahl et al. [1982] also suggested a similar approach based on their results of relocating earthquakes in the Central Aleutians.

Earthquakes. The 550 local earthquakes recorded by the Shumagin network during 1982 are shown in Figure 1. The 12 earthquakes that were selected from the 1982 data set for this detailed study are of sufficient magnitude to show clear onsets of P and S arrivals at most of the 17 stations in the Shumagin network.

The Shumagin seismic network consists of 17 short-period, high-gain seismic stations whose signals are transmitted via radio links to the central recording site at Sand Point (SAS in Figure 1). Five stations are equipped with three-component seismometers. At Sand Point the signals are digitized at a rate of 100 samples/s, and up to 32 channels can be recorded by the nine-track digital (12 bit) tape recorder. An on-line digital event detector monitors 12 channels, and if an event is declared, the detector starts the tape recorder. During event recording, a time code (date and time, UT) from a satellite receiver is injected into the multiplexed data stream at 1-s intervals. The digital seismic data are analyzed at Lamont-Doherty Geological Observatory using interactive computer graphics that allow timing accuracies of 0.01 s.

The selected hypocenters were required to be located within the Shumagin network except for hypocenters with depths greater than 150 km. These were all located due north of the network. An attempt was also made to find earthquakes representing each focal mechanism of the C through F type as defined by Reyners and Coles [1982]. During the final stages of this study, three more earthquakes were added to the set of 12 to satisfy this goal. The initial hypocenters of the 15 earthquakes included in this study are shown as solid circles in the depth section in Figure 1.

The selected earthquakes were located initially using the computer program HYPOINVERSE [Klein, 1978], incorporating a flat-layered velocity structure (H. Rowlett and K. Jacob, personal communication, 1974) (see also Reyners and Coles [1982]). This velocity model (see Table 1) is based on travel times of nuclear explosions detonated in the western Aleutians. The program HYPOINVERSE uses the generalized inverse method called singular value decomposition [Klein, 1978]. The program permits the user to weight arrival times according to quality or distance between the epicenter and a station. No distance weighting was included in this study. P and S arrival times were weighted according to their quality in this study. Further, since S arrival times have a greater slowness along any given ray path than P arrival times, in this study, S arrival times are given weights of 0.25-0.5 when the corresponding P arrivals are weighed 0.5-1.0. These and other standard techniques used in analyzing data from microearthquake networks are treated in detail by Lee and Stewart [1981]. The initial and final hypocentral parameters of the selected earthquakes are listed in Table 2.

TABLE 1. Shumagin Islands Array Velocity Model

P-Wave Velocity of Layer, km s^{-1}	Depth to Top of Layer, km
3.44	0.00
5.56	1.79
6.06	3.65
6.72	10.18
7.61	22.63
7.90	38.51
8.26	90.19

A ratio of P wave velocity to S wave velocity of 1.73 was adopted for all layers.

Three-dimensional ray tracing. The computer program that traces rays through three-dimensional spherical structures was written by Jacob [1970], to study inhomogeneities in P and S velocities of the mantle which are associated with lithospheric slabs. A detailed description of the program is presented by Jacob [1970], and an application of the program for studying anomalous seismic P travel times from the nuclear explosion Longshot, Alaska, is presented by Jacob [1972].

The ray-tracing program uses a stepwise numerical integration by a finite series scheme. Since this numerical scheme requires that the spatial gradient of slowness varies slowly, any sharp discontinuities in slowness are smoothed out to gradient zones over finite distance [Jacob, 1970]. In this study a step size of 2km and a gradient cube of 4km length were used. Therefore the ray-traced ray in Figure 2 is drawn as a smoothed ray. The ray calculated by HYPOINVERSE on the other hand is found by assuming straight-line ray paths within layers of constant velocity.

To form the six models, in all cases a three-dimensional inhomogeneity is prescribed to simulate the subducted slab below the Shumagin Islands region. The inhomogeneity is input into the ray-tracing program. Its basic shape is given as a dipping faceted surface by specifying geographical coordinates of contours of constant depth along the Aleutian arc (see Figure 2).

TABLE 2. Earthquakes That Were Relocated Using Source Delays From Three-Dimensional Ray Tracing

Date	Origin Time	Latitude N	Longitude W	Depth km	Magnitude mb
Dec. 26, 1982	0310:01.95	55°13.51'	160°04.09'	57.00	3.5
Dec. 26, 1982	0310:02.71	55°14.12'	160°02.57'	55.00	3.5
Nov. 27, 1982*	0410:18.28	55°17.02'	160°11.92'	64.00	2.1
Nov. 27, 1982	0410:19.11	55°18.12'	160°10.61'	62.00	2.1
Nov. 10, 1982	0150:55.56	55°04.42'	161°14.48'	69.00	2.2
Nov. 10, 1982	0150:56.30	55°05.35'	161°15.63'	69.00	2.2
Aug. 25, 1982	0851:08.12	55°05.17'	161°04.76'	71.00	1.8
Aug. 25, 1982	0851:08.88	55°06.27'	161°05.59'	72.00	1.8
Oct. 24, 1982	0034:55.22	55°12.65'	161°00.88'	78.00	2.7
Oct. 24, 1982	0034:55.92	55°14.41'	161°01.76'	79.00	2.7
Aug. 26, 1982	1728:54.29	54°59.70'	161°45.49'	100.00	2.7
Aug. 26, 1982	1728:54.93	55°00.54'	161°50.69'	102.00	2.7
Oct. 27, 1982	1927:51.90	55°03.43'	162°00.16'	114.00	2.3
Oct. 27, 1982	1927:52.48	55°06.11'	162°06.38'	118.00	2.3
Sept. 5, 1982	1124:18.05	55°38.18'	161°51.61'	133.00	2.1
Sept. 5, 1982	1124:18.30	55°45.42'	161°58.77'	133.00	2.1
Nov. 5, 1982*	0342:14.08	55°33.55'	161°46.95'	147.00	2.1
Nov. 5, 1982	0342:14.32	55°40.03'	161°53.55'	148.00	2.1
Sept. 9, 1982	1547:45.73	55°33.29'	161°60.00'	156.00	2.3
Sept. 9, 1982	1547:46.07	55°41.03'	162°09.75'	157.00	2.3
Dec. 25, 1982	1014:05.83	55°40.03'	161°51.33'	170.00	2.9
Dec. 25, 1982	1014:05.94	55°50.08'	162°00.34'	173.00	2.9
Sept. 18, 1982	0208:03.50	55°36.98'	161°53.77'	172.00	2.8
Sept. 18, 1982	0208:03.74	55°46.28'	162°05.19'	174.00	2.8
Sept. 4, 1982	1042:41.47	55°55.72'	161°07.90'	176.00	2.0
Sept. 4, 1982	1042:41.76	56°06.44'	161°13.73'	177.00	2.0
Mar. 26, 1982*	0452:43.25	55°53.57'	161°13.42'	184.00	2.3
Mar. 26, 1982	0452:43.44	56°09.54'	161°17.17'	180.00	2.3
July 9, 1982	1547:57.21	55°20.31'	164°08.03'	252.00	4.6
July 9, 1982	1547:57.39	55°32.55'	164°45.65'	245.00	4.6

The first line in a pair is the initial hypocenter; the second is the recalculated hypocenter with respect to the S6 slab model.

*Earthquakes only relocated with respect to the S6 model.

This curved surface, whose numerical representation is given in Table 3, was chosen for this study on the basis of the following criteria: (1) the zero depth contour coincides with the trench axis, (2) the 140km depth contour coincides with the trend of active volcanoes located along the Aleutian arc, and (3) the surface has constant dip of 50° from approximately 100 to 300km depth. To form the variation in models, two parameters, A and B, were used. The slab is given a thickness by specifying a value A to the north and a value B to the south. Both A and B are measured normal to the slab strike but in a horizontal plane (see Figure 2). In the slab models presented below, the value of B was held fixed at 60km, while the position of the upper surface of the slab was varied by choosing A values from 20 to 80 km. When the A value is increased, the slab's surface effectively is moved from south to north, but the geometrical shape of the slab remains the same. The prescribed inhomogeneity has the same structure as the surrounding mantle except for a 7% higher velocity. A velocity contrast of 7% was chosen for this study on the basis of the results of several other studies that have been carried out in the Aleutians (i.e., Jacob [1970, 1972], Engdahl [1973], Fujita et al, [1981], Engdahl et al. [1982], Frohlich et al. [1982], and Spencer and Engdahl [1983]).

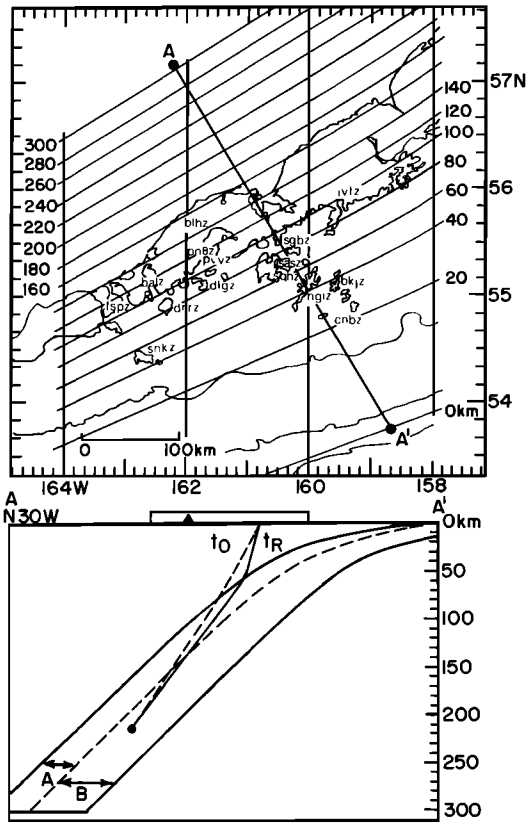

Fig. 2. (Top) A surface projection of the dipping faceted surface that simulates the subducted slab below the Shumagin Islands. The constant depth contours are drawn parallel to the arc, and the depth value is shown on the right for shallow depths and on the left for greater depths. A grid of points is obtained by specifying the latitude, longitude, and depth of the points where a depth contour is intersected by the longitude values (158°, 160°, 162°, and 164°), at 2° intervals of longitude. The A-A' line indicates the position of the cross section shown in the bottom part. (Bottom) The surface that simulates the slab is shown as a dashed line in this cross section. A and B that are measured normal to the slab strike in a horizontal plane are specified to give the slab thickness. The t_R and t_o are schematic ray paths for a three-dimensional traced ray t_R and a ray path t_o calculated through a layered half space by HYPOINVERSE. The difference between the two travel times is the source correction.

Source corrections. Since the computer routine is of the shooting rather than bending type, a large set of rays was shot from a source at depth toward the Shumagin network by looping through an appropriate range of azimuths and takeoff angles at approximately 3°-10° intervals. Travel times between the source at depth and all points of ray emergence at the earth's surface were then also calculated for a flat-layered velocity structure using the travel time subroutines from HYPOINVERSE [Klein, 1978].

Maps of residuals were made by subtracting the ray traced and the HYPOINVERSE travel times and plotting the respective residual value at the point of ray emergence. The source corrections for each station were obtained by interpolating the three residual values closest to each station. When an earthquake is relocated, the station-source corrections that were calculated with respect to its initial hypocenter are input into HYPOINVERSE as station delays, and the program redetermines the hypocenter. The relocation was terminated after one iteration (of the entire procedure of computing source-station corrections and relocating the respective earthquake) since in several test cases the second iteration step only improved the rms residual of the hypocentral solution by 0.01-0.02s and the average relative change in the length of the mislocation vector was less than 5%. For instance, the mislocation vector of the earthquake at 252km depth increased from 41 to 47 km length following a second iteration, while the mislocation vector of the earthquake at 176 km depth increased from 21 to 22.5 km length following a second iteration.

TABLE 3. Latitudes of the Downgoing Slab Model in the Aleutian Island Arc

Depth (km)	Longitude			
	-164.00	-162.00	-160.00	-158.00
0	52.38	52.90	53.35	53.81
40	53.61	54.17	54.69	55.29
80	54.10	54.72	55.28	56.02
120	54.42	55.06	55.70	56.42
160	54.76	55.40	56.07	56.81
200	55.11	55.76	56.45	57.19
240	55.45	56.13	56.83	57.56
280	55.79	56.49	57.21	57.93

Results

The major result of this study consists of improved earthquake hypocenters that are more consistent with the presence of a high-velocity slab than previous locations. The new slab model presented constitutes the best available estimate of the geographical position and geometrical shape of the upper surface of the subducted lithospheric slab beneath the Shumagin network.

Earthquake relocations. Twelve earthquakes are relocated using travel time corrections derived from the six different slab models S2-S8 shown in Figure 3. The models S2-S8 differ in such a way that the upper surface of the slab is moved horizontally toward north 30° west in 10-km increments for models S2-S6, and in a 20-km increment from S6 for model S8. The S6-S8 slab models dip at an angle of 50° toward north 30° west. Initially, a slab model dipping at 60°

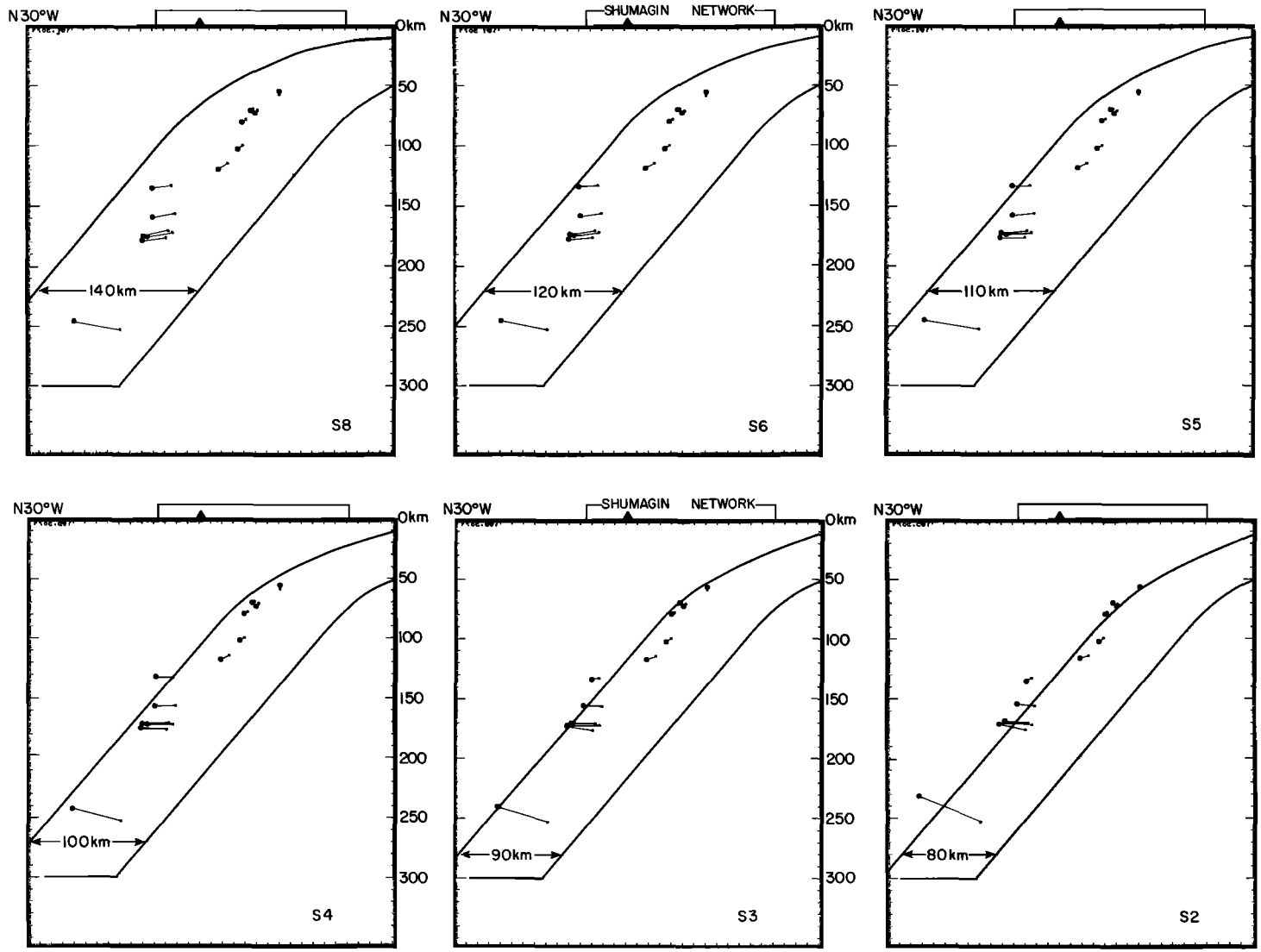

Fig. 3. Depth cross sections taken along the profile A-A' in Figure 1. Initial hypocenters and recalculated hypocenters are shown as small and large solid circles connected by a line. The recalculated hypocenters are determined using the model shown in the respective cross sections, S2-S8. The bracket on top of each cross section indicates the position of the Shumagin network. The triangle on top shows the position of the volcanic axis.

below 120-140 km depth was rejected because hypocenters at depths of 200-250 km tended to relocate north of the slab, while hypocenters at depths shallower than 100 km remained almost stationary, deep within the slab.

In Figure 3, pairs of initial and recalculated hypocenters are shown as a small and a large circle connected by a line. For the S2 model where the slab's upper surface is situated farthest to the south, most of the recalculated hypocenters fall outside the slab. Similarly, in the S3 model many of the recalculated hypocenters fall just north of the slab surface. Hence the S3 model can be considered to be the southernmost end-member of a whole suite of possible slab models. Conversely, the S8 model probably is located somewhat farther north than a most likely northerly end-member of possible slab models. When the S8 model is used, all of the recalculated hypocenters are located well within the slab, and all except one of the mislocation vectors dip downward. Since the 7% higher velocity of the slab is replacing the regular velocity structure, the net effect is to increase the depth of the hypocenters. Rays traced through the S8 model almost do not sense the refracting effect of the dipping interface, and the relative difference in the station delays is less than for the other models. Since most of the hypocenters fall within the respective slab model in the S4, S5, and S6 models, it is not clear from the plotted hypocenters in Figure 3 what model gives a best fit. To select a best fitting model, a quantitative comparison of the computed and observed arrival time patterns is needed.

The initial and recalculated epicenters for the S6 model are shown in map view in Figure 4. Within the Shumagin network at depths above 100 km the initial and recalculated hypocenters almost coincide. Near the edges and to the north of the network, for earthquakes deeper than 100 km the size of the mislocations increases with distance away from the center of the network. It is worthwhile to point out that 70-80% of the seismicity recorded by the Shumagin network occurs above 100 km depth and hence is not mislocated significantly due to slab effects.

To evaluate which of the S2-S8 models gives a best fit to the recorded travel times, the calculated rms travel time residual for P and S arrivals of each earthquake is plotted versus the respective model in Figure 5a. Although the calculated rms values appear to be only weakly model dependent, a fairly consistent pattern emerges. Shallow local minima in the rms curves suggest that the shallower hypocenters (less than 130 km) are more compatible with models such as S3 or S4 than, for example, S6 or S8 models. Conversely, the deep hypocenters (greater than 130 km) appear to be more consistent with the S5 or S6 models. Hence these comparisons of rms values suggest that a model fitting S4 at shallow depth (since most of the recalculated hypocenters fall outside the slab in models S2 and S3) and S6 at 250 km depth is most consistent with the arrival time data. It is worth pointing out that the different models result in mislocation vectors that have weak local minima which approximately coincide with similar changes in the rms values (Figure 5b). The variations in the mislocation vectors, however, cannot be used as a criterion to select a best fitting model.

When the source corrections are included in the earthquake location procedure, the resolution of the velocity structure is enhanced. Backus and Gilbert [1970] demonstrated that there is a trade-off between the resolution and the statistical errors that in this case are the rms values. Their results indicate that the statistical error can only be reduced at the expense of a degradation in resolution and vice versa. Hence the rms values of the hypocenters that are based on source corrections cannot be easily compared with the rms values calculated without source corrections since the resolution differs in these two cases. It is nonetheless meaningful to compare rms values of the models S2-S8 since they all have the same resolution.

Wave forms and ray paths. The ray-tracing program can be used not only to calculate travel times but also to look for regions of ray focusing or defocusing. In regions of complex velocity distribution the amplitudes of transmitted waves and the generation of coda waves following the P wave can vary significantly, depending on the ray path [Richards and Menke, 1983]. Hence the frequency content and shape of the seismograms may supply additional criteria for selecting a best fitting slab model, although quantitative modeling of the observed waveforms and coda is beyond the scope of this paper.

To demonstrate that the seismograms used in this study show significant variations in waveform character depending on the path, sample record sections of an earthquake at 156 km depth is shown in Figure 6. The record sections that are intended to show phase arrivals and qualitative variations in frequency content of the whole seismogram are normalized to approximately the same maximum peak to peak amplitude except those for the station FSP. The station FSP has a high background noise level and is operated at a lower gain than the other stations in the network. A map view of the epicenter and the station distribution is shown toward the left, and two sample depth cross sections (B-B') that are ray traced for the models S3 and S4 are also shown. The S4 model is more consistent than the S3 model with the observed average relative amplitudes that are shown as bars on top of the cross sections. The average relative amplitudes observed at stations such as SNK or CNB do not support the strong shadow zone implied by model S3. When comparing those amplitudes with amplitudes of stations located near the volcanic axis such as DLG or PVV, the amplitudes are more consistent with model S4. Further, the S4 model suggests that stations SNK and DRR should be recording rays with most of their path length within the slab. Hence it is noteworthy that the stations SNK and DRR have smaller P amplitude but more high-frequency coda following the P wave than stations located on the Alaska Peninsula such as DLG, FSP, PS4, PN6, or BLH. A similar pattern is observed along the profile A-A' to the right in Figure 6 where stations such as SAS, BKJ, and CNB are in a shadow zone in model S3 but receive rays traveling up the slab in model S4. These stations also observe more high-frequency coda

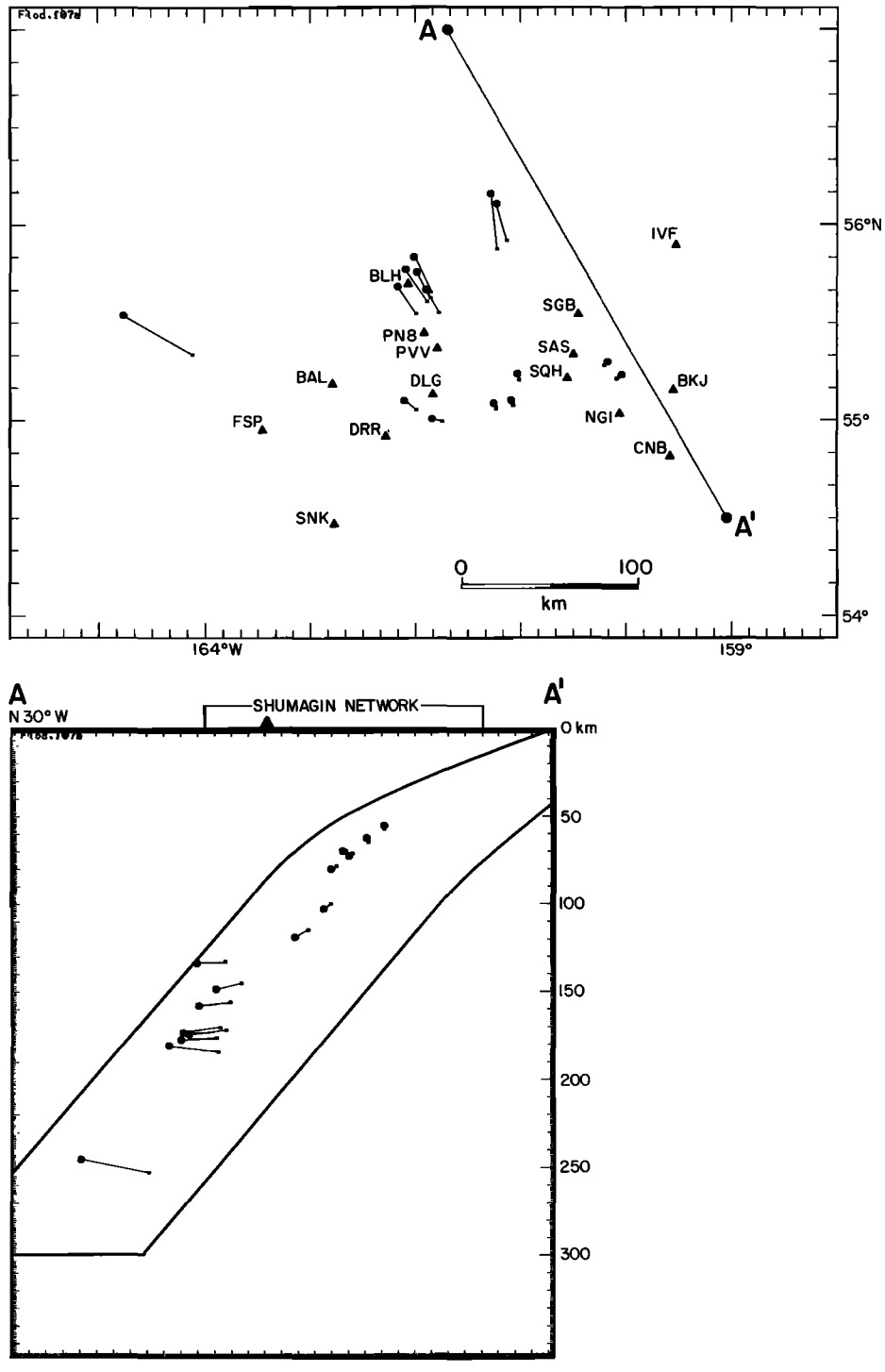

Fig. 4. Initial and recalculated hypocenters (with respect to the S6 model) are shown in map view and cross section. Note the size increase of mislocation vectors with depth and toward the north.

than stations such as PS1 and BLH, recording almost vertical rays that travel through the overriding plate.

The seismograms in Figure 6 also show several prominent features that are not analyzed in this study. For instance, the stations located along the volcanic arc record very low S/P amplitude ratios that are similar to the ones observed by Matumoto [1971] near Mount Katmai, Alaska. In some of the seismograms possible S-Sp (e.g., see station SNK) or P-Ps converted phases can be seen, as has been suggested by Reyners [1980], who studied microearthquakes in the slab beneath New Zealand. The large station spacing of 40-50 km in the Shumagin network, however, makes it difficult to identify these secondary arrivals at

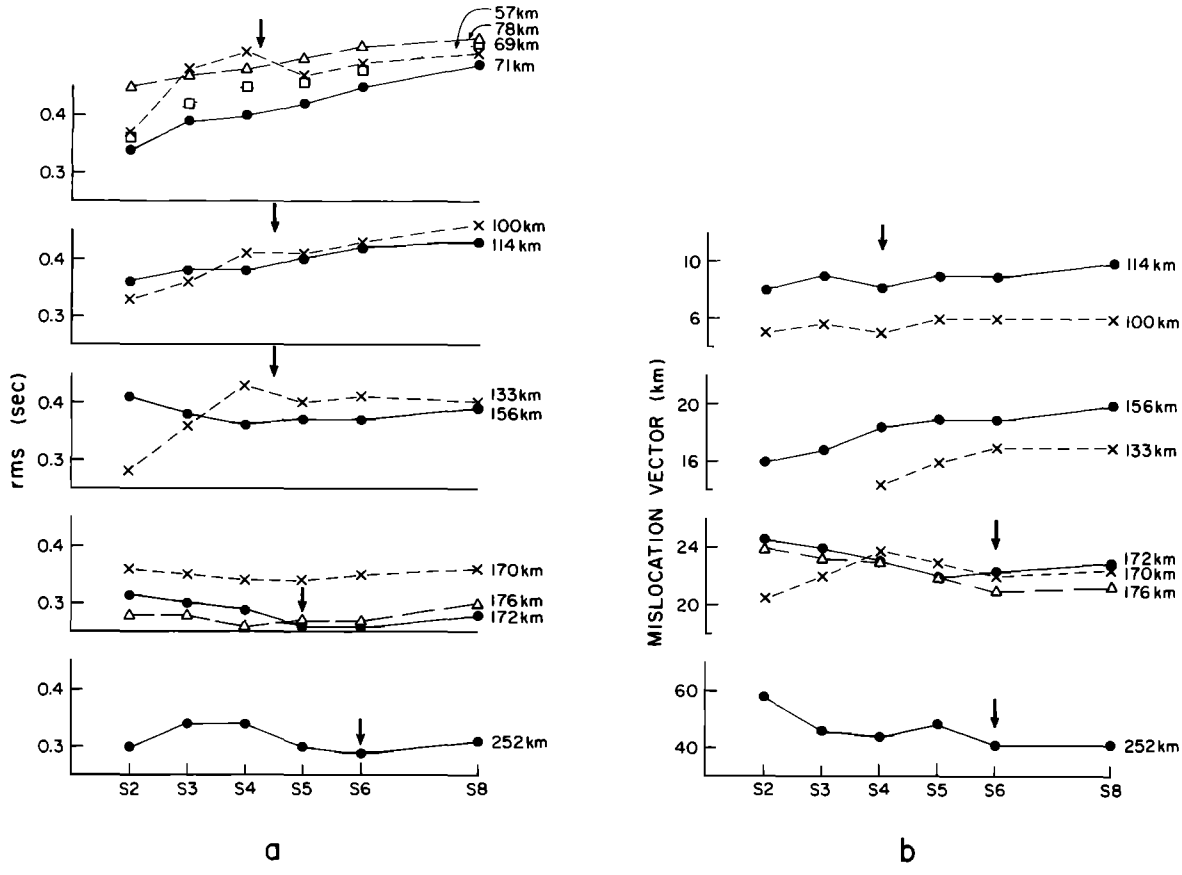

Fig. 5. (a) The rms residual of the recalculated hypocenter solutions from HYPOINVERSE plotted versus model type. The initial depth of each hypocenter is shown toward the right. (b) Mislocation vector measured from the cross sections in Figure 2 normal to the slab plotted versus model type. The initial depth of each hypocenter is shown toward the right. The arrows indicate the positions of shallow minima.

adjacent stations. The observed S-P times along the A-A' profile indicate in some cases either that the S arrival is preceded by converted phases or that the Vs/Vp velocity ratio is path dependent.

Similar combinations of record sections and ray-tracing cross sections, as shown in Figure 6, were created for eight earthquakes located at different depths from 70 to 250 km. The results of comparing the amplitudes of transmitted waves and the path dependence of the coda with the ray-tracing profiles indicate that S3 or S4 models fit the waveforms of the shallow earthquakes and that S5 or S6 fit the waveforms of the deep earthquakes below 170 km depth.

The plate interface. The relative local minima in the curves of rms residual values in Figure 5 and the results of comparing ray-tracing profiles with waveforms are used to derive a best fitting model, FS6. This best fitting model is shown in Figure 7 along with the S6 model and the envelope (RC) of the upper surface of the hypocentral cross sections presented by Reyners and Coles [1982]. The FS6 model has a dip of 45° toward north 30° west at depths below 80 km. In comparison, within the same depth range the S2-S8 models dip at an angle of 50°, while the RC envelope dips at 60° below 150 km depth. For the FS6 model the position of the slab is best constrained in the range from 60 down to 220 km depth. Above 60 km depth, no earthquakes were relocated, and hence no additional constraints were obtained concerning the exact position of the main thrust zone.

The position of the main thrust zone as shown in Figure 7 was determined by interpolating a smooth curve between the trench axis and the position of the interface as determined by the most shallow hypocenters. Beneath 220 km depth the interface is extrapolated downward since only a handful of the rays shot from the 252-km-deep hypocenter exit the slab's upper surface below 220 km depth. The lower surface of the subducting slab is not shown in Figure 7 since no calculated rays are observed to cross the lower surface, and hence its position remains unknown.

In Figure 7 a contour map of equal depth lines that represent the upper surface of the slab for model FS6 is shown. The 0-km depth contour falls along the trench axis and the 100-km depth contour coincides with the volcanic front. The increase in width between the contours of constant shallow depth reflects the widening of the shallow thrust zone, as described by Davies and House [1979]. The parallel and equidistant depth contours below 80 km depth reflect the

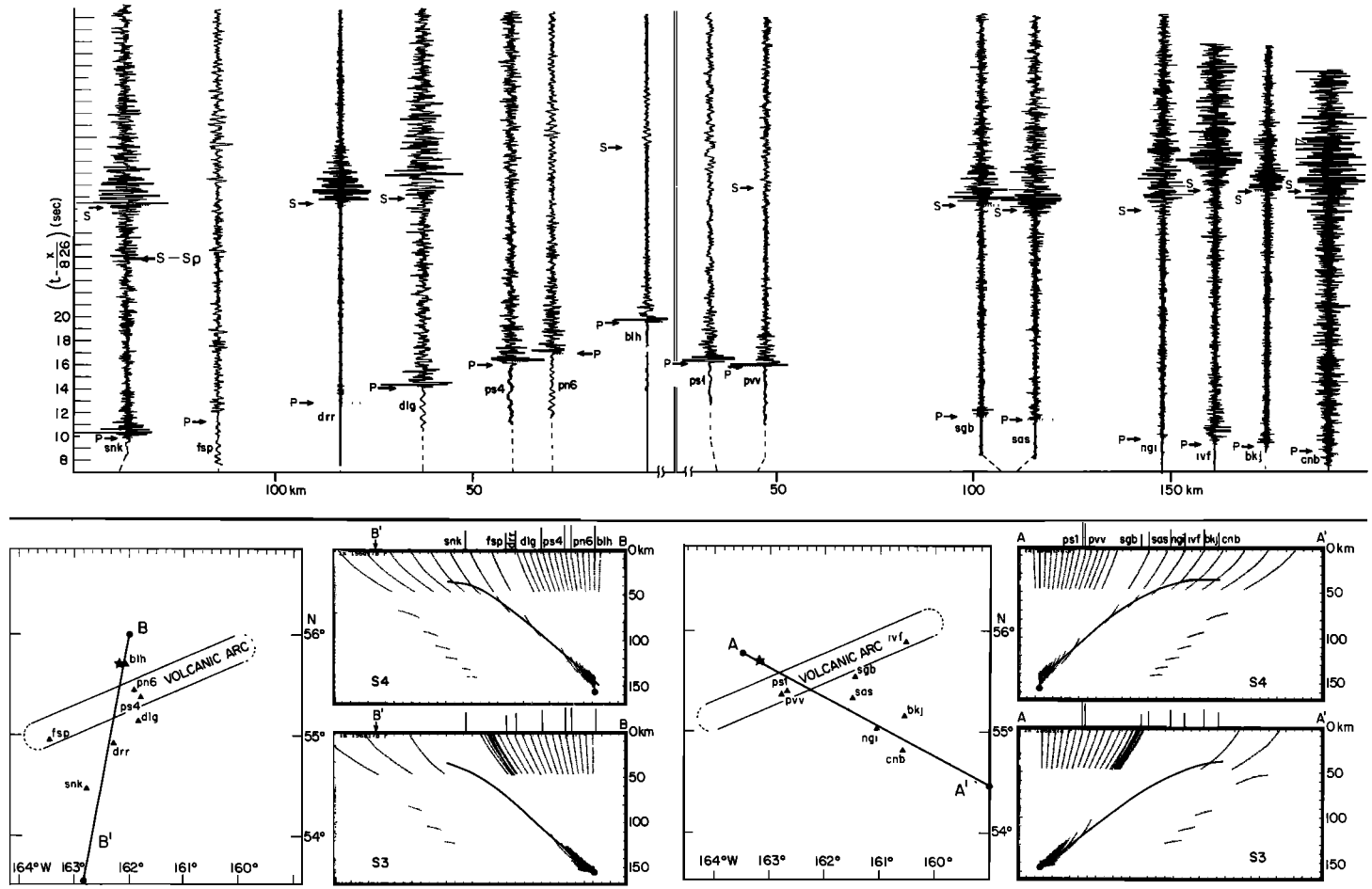

Fig. 6. (Top) A record section of an earthquake (that occurred September 9, 1982; see Table 2) with a relocated hypocentral depth of 156 km. The reduction velocity of 8.26 km/s is the half-space velocity in the Rowlett and Jacob velocity structure. Arrivals of P and S waves are indicated and stations are designated by a three letter code. (Bottom center left) Depth cross sections B-B' which were ray traced along a constant azimuth; when rays pass through a velocity gradient zone, they are plotted as a dotted curve. Note, that rays are shown as they pass out of the upper or lower surface of the slab and through the crust. The upper surface of the slab is shown as a curved heavy line; on top of each cross section the length of the vertical bar is proportional to the local magnitude. In map view the epicenter is shown as a star and seismic stations as triangles. Note that rays traveling up the slab are observed in the S4 model but not in the S3 model. (Bottom right) Depth cross sections along the profile A-A' from the same source but taken along an azimuth toward southwest.

constant dip of the downgoing slab at these depths.

Relocation using grid delays. Since calculating source corrections for every earthquake recorded by the Shumagin network would be both uneconomical and time consuming, a preliminary grid of source corrections has been calculated. The grid was selected such that it forms a surface located 20 km inside (as measured from the top surface) the S6 model. Rays were traced through the S6 model, and source corrections relative to each grid point were determined for each station, as is shown in Figure 8. The S6 model was chosen since it appears to be most consistent with the deeper earthquakes, whose hypocenters are more sensitive to the chosen model than those of the shallower earthquakes. The density of points in the grid that was limited by the available computing resources was chosen to give sufficient coverage of the slab and to minimize possible artifacts caused by a too dispersed grid. Linear distance weighting was used to interpolate between the fixed grid points to compensate for the large grid spacing.

To check the reliability of the grid delays, the 12 events relocated with respect to the models S2-S8 were relocated with respect to the grid. Since a ray starting point in this case is located closer to the upper surface of the slab (than an initial location used previously), the relocated hypocenters have mislocation vectors of similar size, as found by performing two iterations of the ray-tracing relocation method.

Source corrections based on this preliminary grid were used to recalculate all the 1982 hypocenters that are deeper than 50 km (see Figure 9). Several significant changes are observed in the distribution of hypocenters. When comparing Figures 1 and 9, the most prominent changes are the absence of the apparent increase in the dip of the slab around 100-150 km depth and the shallowing of the dip of the Benioff zone.

The cluster of the recalculated hypocenters between 140-170 km depth is now aligned with the general trend of hypocenters at shallower depths. In map view the corresponding epicenters no longer fall along the volcanic axis but are located 30-50 km to the north of the volcanoes.

This preliminary grid is not dense enough to improve the resolution of the double-planed Benioff zone. A set of two parallel grids spaced 30-40 km apart may provide an improved resolution. Each grid may have to consist of 200-300 points to make possible uncertainties caused by grid coarseness less than 0.1 or 0.2 s. The grid coarseness may also cause a few of the earthquakes to be located just outside the upper surface of the FS6 slab model (see Figure 9).

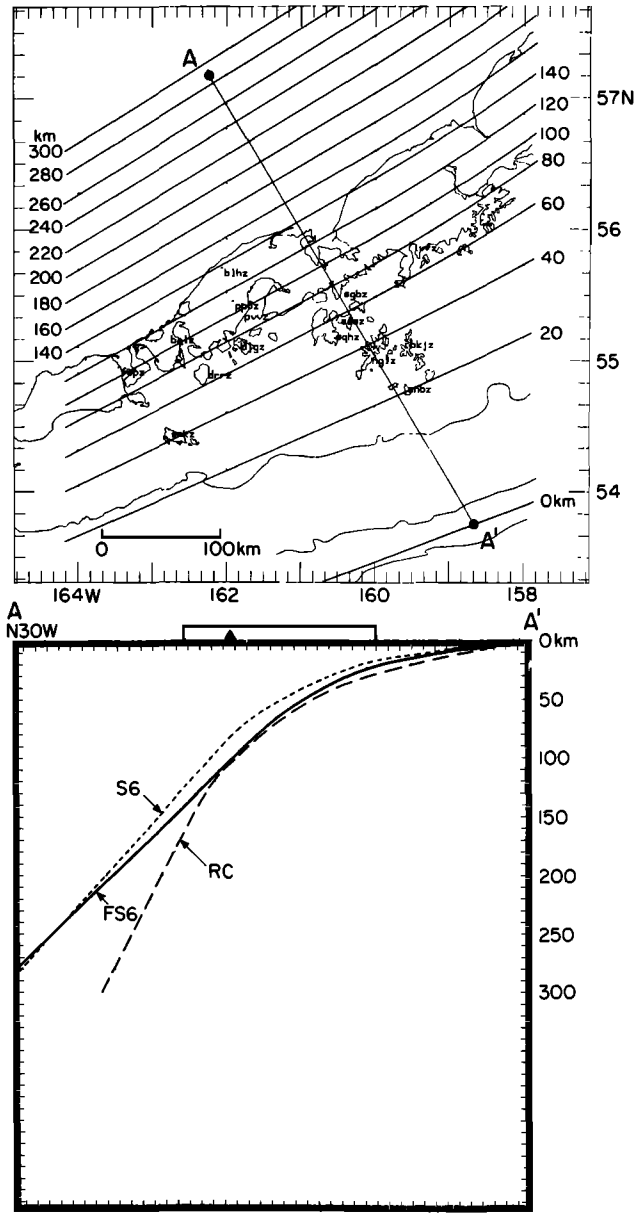

Fig. 7. The FS6 slab model shown as contours of equal depth and in depth cross sections. For comparison the S6 model is included (in the depth section) as well as the upper envelope (RC) of the hypocentral distribution shown by Reyners and Coles [1982].

Discussion

Slab velocity contrast. The slab models presented in this study have a constant 7% higher velocity than the surrounding mantle. A constant percentage, regardless of depth, does not reflect the detailed thermal structure of the slab very accurately. In the case of the FS6 model in Figure 7 the upper surface of the slab can be considered to represent a trajectory of subduction for a particle initially located near the surface of the oceanic crust. An isotherm would be expected to migrate into the slab as the slab penetrates farther down into the mantle [Toksoz et al., 1971]. Therefore if the occurrence of earthquakes is in part controlled by the thermal structure of the slab, it is not unreasonable to expect that the deeper earthquakes gradually trend into the slab, away from the upper surface of the slab [House and Jacob, 1982]. Such a trend of hypocenters with depth into the slab is observed in this study (see Figure 4) and several other similar studies [e.g., Spencer and Engdahl, 1983].

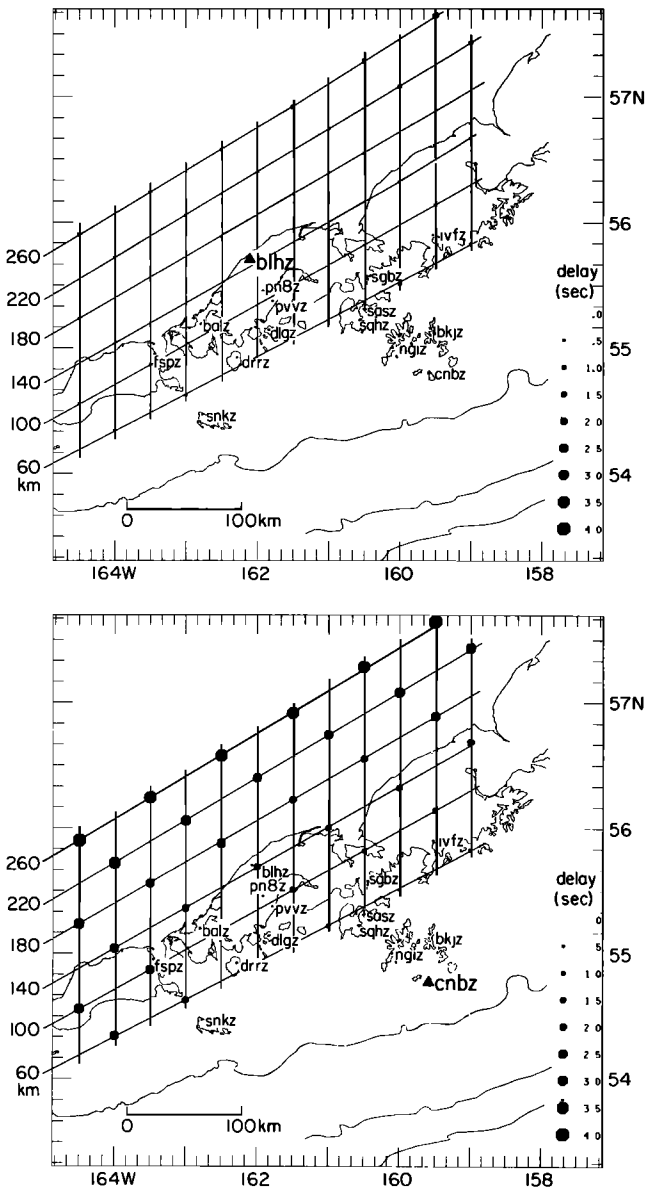

Fig. 8. (Top) A grid of source corrections used to relocate the 1982 hypocenters. The size of the octagons at each grid point is proportional to the source correction observed at station BLH. (Bottom) Same as above except here the size of the octagons at each grid point is proportional to the source correction observed at station CNB.

If a velocity contrast lower than 7% had been used, then the recalculated trend of hypocenters would have been more steeply dipping. Alternatively, for example, a 10% velocity contrast or a scenario of a 2% low velocity wedge located above the slab of 7% higher velocity (than the surrounding mantle) would have resulted in a less steeply dipping slab. To explain a velocity contrast of the order of 7%, Jacob Huppert and Frohlich [1981] point out that the material in the downgoing slab may be up to 700°C cooler than the surrounding mantle. Such a temperature contrast, however, can cause at most 5% velocity contrast. To obtain an additional velocity contrast as high as 4%, Jacob [1972] and Huppert and Frohlich [1981] argue that 0.001 fraction of partial melt in the mantle outside the subducted slab is needed.

Slab surface. Hasegawa et al. [1978] used ScSp converted phases to obtain an independent constraint on the position of the upper surface of the slab under northern Honshu in Japan. When the seismicity was relocated using source corrections from three-dimensional ray tracing, the hypocenters were located approximately 10 km below the boundary of the slab. In the Shumagin region, no such independent constraints are available yet. The observed difference in the character of seismograms recorded by the Shumagin network, however, supports indirectly the interpretation that the earthquakes are located 10–20 km below the surface of the slab. The conversion of transmitted P waves into possible converted phases and high-frequency coda waves suggests a travel path through highly heterogeneous structures, perhaps from fracturing or from alternating layers of different velocity [e.g., Menke and Richards, 1983; Aki, 1982].

McAdoo et al. [1978], who modeled the outer bulge in the Kuriles assuming an elastic-plastic lithosphere under horizontal compression, point out that their elastic-plastic lithosphere is overlain by 10–20 km of tensionally incompetent crust. This highly block-faulted layer is created during the formation of the outer bulge and the passing of the slab into the trench. Such a layer that does not support large deviatoric stresses and has been accreted onto the plate again during subduction may explain the observed generation of high-frequency coda and is also consistent with having the earthquakes located within the slab.

Slab dip. The slab dips from the trench beneath the Shumagin network region at a shallow angle of 10° - 15° down to depths of 40–50 km. In this depth range the coupling between the two plates is interpreted to be elastic-brittle on the basis of the occurrence of great earthquakes along the plate boundary [Davies et al., 1981]. The absolute value of the dip in this depth range has been interpreted to be influenced by the age of the subducting lithosphere and the rate of plate convergence [Ruff and Kanamori, 1980].

An increase in the dip of the slab up to 45° is observed at depths of 50–80 km beneath the Shumagins (see Figure 7). Jacob et al. [1977] proposed that this change in dip is related to the increase in the density of the downgoing plate. They point out that an effective increase in density within the subducted mass can result from processes such as removal of possibly subducted sediments from the slab, dehydration of the oceanic crust, or phase changes. Further, the steeper dip may be related to decoupling of the descending plate and hence may explain the absence of great thrust earthquakes below 40–60 km depth in the Aleutians [Jacob et al., 1977; House and Jacob, 1983].

The FS6 model indicates that the region around 100 km depth is unbending (see Figure 7) and thus the upper (northerly) portion of the slab should be characterized by compressive stresses. In earlier studies this region was considered to bend downward and thus should have been

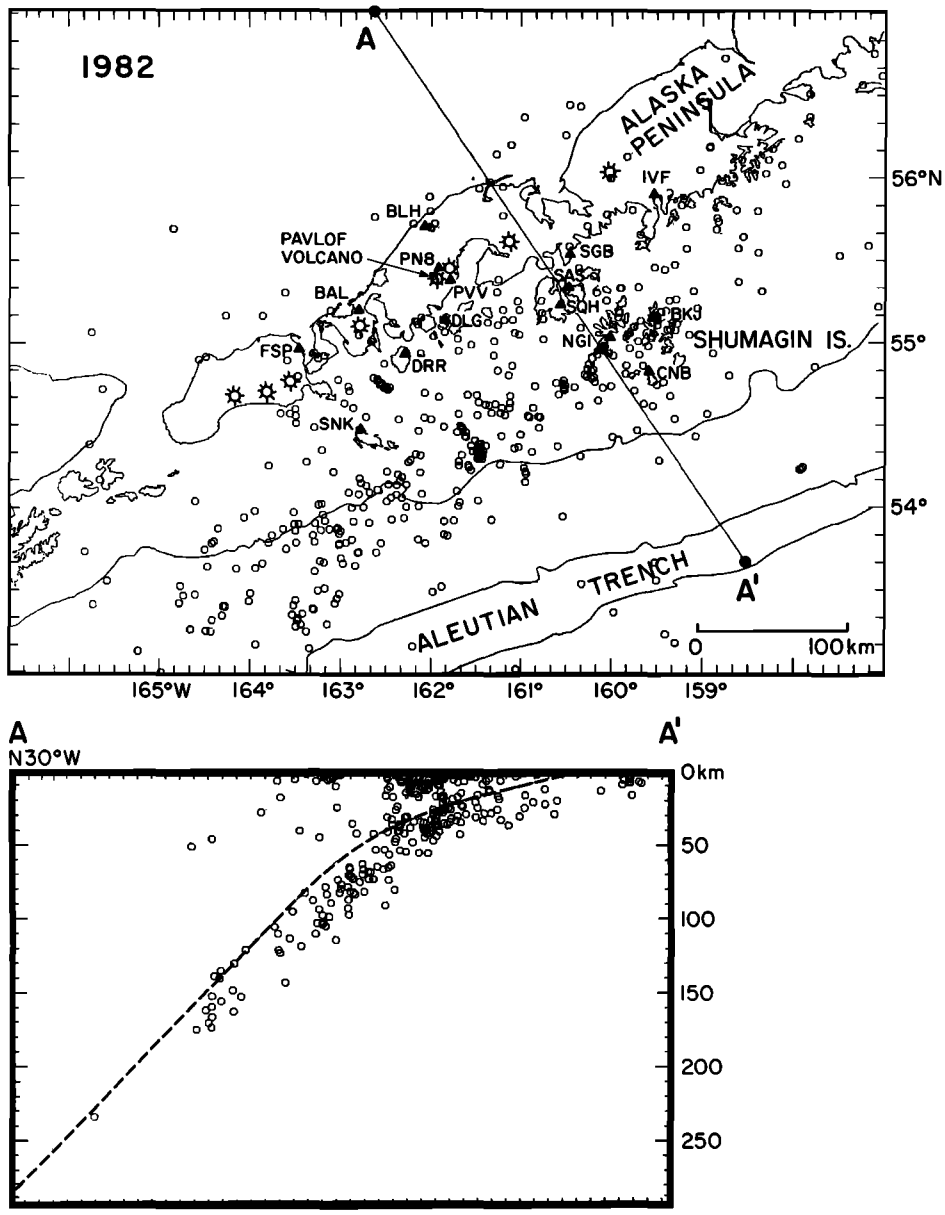

Fig. 9. The 1982 Shumagin seismicity relocated using the grid of source corrections as shown in Figure 8. (Top) Map view showing epicenters as open circles and seismic stations as solid triangles. Active volcanoes on the Alaska Peninsula are shown as marked open circles. (Bottom) Depth cross section with no vertical exaggeration taken along the profile A-A'. The dashed line indicates the position of the upper surface of the FS6 slab model.

tensional. The magma generation was interpreted to be indicative of further removal of lighter volatile or hydrous components from the slab. Consequently, further decoupling was occurring in this region, and the slab was sinking into the hot asthenosphere (i.e., Jacob et al. [1977]). The results presented here indicating a straight plate do not require such a mechanism. Instead, they suggest that some internal stresses cause unbending of the slab in the 100-km depth range where the mantle surrounding the slab is characterized by low-velocity, low-Q zone. Alternatively, the resulting dip of the slab may be influenced by mantle convection (i.e., Tovish et al. [1978]), and the magma generation may be more related to the slab petrology and the presence of hydrous minerals than to the detailed shape of the slab.

The best fitting slab model, FS6 provides new constraints on the position and geometry of the plate interface beneath the Shumagin Islands, Eastern Aleutians. In the future, joint hypocentral relocations and velocity inversions may yield more detailed information about the plate interface in the 20–100 km depth range. Combined land-based and ocean bottom seismograph experiments may reveal the interface at shallower depths. Unraveling the deep structure below 100

km is critically dependent on the availability of regional and teleseismic data. Identification of converted phases combined with three-dimensional ray tracing may provide a useful tool in this respect. Further refining of the available models of the plate interface between the North American plate and the Pacific plate will contribute to the understanding of both general plate tectonics and the occurrence of earthquakes and volcanic activity along the Aleutian arc.

Conclusions

Relocating 12 different earthquakes (using arrival times recorded by the Shumagin seismic network) with respect to six different models of the downgoing slab in the eastern Aleutians by using three-dimensional ray tracing provides the following results.

A previously observed apparent increase in dip of the subducted slab at depths of ≈100 km disappears. The depth range around 100 km appears to be a region of slab unbending, and hence this may raise the question whether the processes of unbending and magma generation are related.

Earthquakes located within the Shumagin network at depths less than 100 km in most cases have mislocation vectors that are less than 2-4 km when the effect of the slab is included.

Earthquakes located to the north of the Shumagin network at depths greater than 100 km can be significantly mislocated if slab effects are not taken into account. For instance, a 250-km-deep earthquake was found to be displaced 40 km to the northwest when the effect of the slab was included.

The subducted slab can be modeled as a structure that dips at a constant angle of 45° toward north 30° west at depths between 80 and 250-300 km and has a velocity 7% higher than the surrounding mantle. This model is consistent both with shallow local minima in the rms values of the hypocenter solutions and the observed waveform character of recorded seismograms. This result is also supported by the whole set of 1982 earthquakes when their hypocenters are recalculated using a set of source corrections determined for a grid of points positioned near the upper surface of the slab model. Finally, rays that propagate a considerable distance through the root zone of the volcanic arc and through the aseismic wedge, above the dipping slab, have very low S to P amplitude ratios. Hence in these regions the crust or upper mantle seems to attenuate S waves very effectively.

Acknowledgments. The manuscript was read critically by L. Jones, K. Jacob, C. Nicholson, and G. Suarez. Valuable comments were provided by R. Cockerham and W. A. Prothero, Jr. The author would like to thank K. Jacob for giving helpful suggestions and encouragement and for making the three-dimensional ray-tracing programs available. Thanks are due to S. Rosen and M. Luckman, who located the 550 earthquakes recorded during 1982. D. Johnson and L. Skinta provided the technical effort that was needed to keep nearly all of the Shumagin network stations operating during 1982. L. Niebur and S. Turnbow typed the manuscript, and K. Nagao and M. Luckman drafted the figures. This work was supported by the U.S. Department of Energy (contracts DE-AC02-76ERO-3134 and DE-FG-02-84-ER13221). Lamont-Doherty Geological Observatory contribution 3707.

References

Aki, K., Scattering and attenuation, Bull. Seismol. Soc. Am., 72, S319-S330, 1982.

Backus, G., and F. Gilbert, Uniqueness in the inversion of inaccurate gross earth data, Philos. Trans. R. Soc. London Ser. A, 266, 123-192, 1970.

Davies, J. N., and L. House, Aleutian subduction zone seismicity, volcano-trench separation, and their relation to great thrust-type earthquakes, J. Geophys. Res., 84, 4583-4591, 1979.

Davies, J., L. Sykes, L. House, and K. Jacob, Shumagin seismic gap, Alaska Peninsula: His-tory of great earthquakes, tectonic setting, and evidence for high seismic potential, J. Geophys. Res., 86, 3821-3856, 1981.

Engdahl, E. R., Relocation of intermediate depth earthquakes in the central Aleutians by seismic ray tracing, Nature Phys. Sci., 245, 23-25, 1973.

Engdahl, E. R., J. W. Dewey, and K. Fujita, Earthquake location in island arcs, Phys. Earth Planet. Inter., 30, 145-156, 1982.

Frohlich, C., S. Billington, E. R. Engdahl, and A. Malahoff, Detection and location of earthquakes in the central Aleutian subduction zone using island and ocean bottom seismograph stations, J. Geophys. Res., 87, 6853-6864, 1982.

Fujita, K., E. R. Engdahl, and N. H. Sleep, Subduction zone calibration and teleseismic relocation of thrust zone events in the central Aleutian Islands, Bull. Seismol. Soc. Am., 71, 1805-1828, 1981.

Hasegawa, A., N. Umino, and A. Tokagi, Double-planed deep seismic zone and upper-mantle structure in the northeastern Japan arc, Geophys. J. R. Astron. Soc., 54, 281-296, 1978.

House, L. S., and K. H. Jacob, Thermal stresses in subducting lithosphere can explain double seismic zones, Nature, 295, 587-589, 1982.

House, L. S., and K. H. Jacob, Earthquakes, plate subduction, and stress reversals in the eastern Aleutian arc, J. Geophys. Res., 88, 9347-9374, 1983.

Huppert, L. N., and C. Frohlich, The P velocity within the Tonga Benioff zone determined from traced rays and observations, J. Geophys. Res., 86, 3771-3782, 1981.

Jacob, K. H., Three-dimensional seismic ray tracing in a laterally heterogeneous spherical earth, J. Geophys. Res., 75, 6675-6689, 1970.

Jacob, K. H., Global tectonic implications of anomalous seismic P travel times from the nuclear explosion Longshot, J. Geophys. Res., 77, 2556-2573, 1972.

Jacob, K. H., K. Nakamura, and J. N. Davies, Trench-volcano gap along the Alaska-Aleutian arc: Facts and speculations on the role of terrigenous sediments for subduction, in

Island Arcs, Deep Sea Trenches, and Back-Arc Basins, Maurice Ewing Ser., vol. 1, edited by M. Talwani and W. C. Pitman III, pp. 243-258, AGU, Washington, D. C., 1977.

Klein, F. W., Hypocenter location program HYPOINVERSE, part 1, Users guide to versions 1, 2, 3, and 4; part 2, Source listings and notes, U.S. Geol. Surv. Open File Rep, 78-694, 114 pp., 1978.

Lee, W. H. K. and S. W. Stewart, Principles and Applications of Microearthquake Networks, 293 pp., Academic, Orlando Fla., 1981.

Matumoto, T., Seismic body waves observed in the vicinity of Mt. Katmai, Alaska, and evidence for the existence of molten chambers, Geol. Soc. Am. Bull., 82, 2905-2920, 1971.

McAdoo, D. C., J. G. Caldwell, and D. L. Turcotte, On the elastic-perfectly plastic bending of the lithosphere under generalized loading with application to the Kurile Trench, Geophys. J. R. Astron. Soc., 54, 11-26, 1978.

Menke, W., and P. G. Richards, The horizontal propagation of P waves through scattering media: Analog model studies relevant to long-range Pn propagation, Bull. Seismol. Soc. Am., 73, 125-142, 1983.

Minster, J. B., and T. H. Jordan, Present-day plate motions, J. Geophys. Res., 83, 5331-5354, 1978.

Reyners, M., A microearthquake study of the plate boundary North Island, New Zealand, Geophys. J. R. Astron. Soc., 63, 1-22, 1980.

Reyners, M., and K. Coles, Fine structure of the dipping seismic zone and subduction mechanics in the Shumagin Islands, Alaska, J. Geophys. Res., 87, 356-366, 1982.

Richards, P. G., and W. Menke, The apparent attenuation of a scattering medium, Bull. Seismol. Soc. Am., 73, 1005-1021, 1983.

Ruff, L., and H. Kanamori, Seismicity and the subduction process, Phys. Earth Planet. Inter., 23, 240-252, 1980.

Sleep, N. H., Teleseismic P-wave transmission through slabs, Bull. Seismol. Soc. Am., 63, 1349-1373, 1973.

Spencer, C. P., and E. R. Engdahl, A joint hypocenter location and velocity inversion technique applied to the central Aleutians, Geophys. J. R. Astron. Soc., 72, 399-415, 1983.

Toksoz, M. N., J. W. Minear, and B. R. Julian, Temperature field and geophysical effects of a downgoing slab, J. Geophys. Res., 76, 1113-1138, 1971.

Tovish, A., G. Schubert, and B. P. Luyendyk, Mantle flow pressure and the angle of subduction: Non-Newtonian corner flows, J. Geophys. Res., 83, 5892-5898, 1978.

E. Hauksson, Department of Geological Sciences, University of Southern California, Los Angeles, CA 90089-0741

(Received November 21, 1983;
revised July 13, 1984;
accepted August 1, 1984.)